

The class II BF-37°C-2D22-NGC structure may represent a structure trapped at an intermediate stage of expansion at 37°C. Previous cryo-EM studies of the uncomplexed 37°C DENV2(NGC) sample showed four stages of structural change (9), of which only stage 1 and 3 structures were interpreted. The first stage is similar to the unexpanded structure. The third stage showed that all dimers had moved to a higher radius. The A-C dimer rotated, whereas the B-B' dimer dissociated from each other. Comparison of the class II BF-37°C-2D22-NGC structure with the DENV2 37°C stage 3 structure (Fig. 3B, ii) showed similar organization to that of the A-C dimers. The B-B' dimer, on the other hand, seemed to be a transitional structure between the DENV2 NGC 37°C stage 1 and 3 structure, as it lay at a radius in between these two structures (Fig. 3B, i and ii).

The ~21 Å resolution class II AF-37°C-2D22-NGC cryo-EM map (Fig. 4, A and B, and fig. S10) showed clear Fab densities near the fivefold vertices and much weaker Fab densities near the threefold vertices. The E protein densities were sparse; therefore, the map was not interpreted. The positions of Fab density near the fivefold vertices was similar to those in the BF-37°C-2D22-NGC map, but not those near the threefold vertices. The Fab densities near the fivefold and threefold vertices probably represent those that are bound to each end of the A-C' dimer. Neutralization profiles of BF-37°C-2D22-NGC and AF-37°C-2D22-NGC samples were similar (fig. S12B), suggesting that the poor Fab density near the threefold vertices may be due to local movement in the structure rather than low Fab occupancy.

DENV fusion in endosomes requires E protein dimers to disassociate and then reassociate into trimeric structures. Fab 2D22 locks both ends of all dimers on DENV2(PVP94/07), thereby preventing E protein reorganization. In the BF-37°C-2D22-NGC and AF-37°C-2D22-NGC samples, only two-thirds of the dimers on the virus surface are locked. The remaining free dimer in each raft is probably unable to form trimers. Indeed, HMAb 2D22 effectively neutralized DENV2 strains PVP94/07 and NGC, even though the latter bound one-third fewer antibody molecules (fig. S12A).

Many human antibodies that strongly neutralize dengue bind to quaternary epitopes (epitopes involving more than one E protein molecule) (6, 11, 12). Human antibodies that neutralize DENV serotypes 1 and 3 bound to quaternary epitopes, which require virion assembly (11, 12). In contrast, HMAb 2D22 binds to a simpler epitope that requires only the formation of E homodimers. Several DENV serotype cross-neutralizing human antibodies (13) were also shown to bind E protein dimer epitope (EDE) (fig. S13, B, C, and D). These EDEs are largely similar to 2D22 epitope (fig. S13, A, B and C). Compared to HMAb C8 and C10 (fig. S13, A, B, and C), HMAb 2D22 has more interactions on DIII that are unique to DENV2 (fig. S13E), leading to its serotype specificity.

The DENV2 surface is more dynamic than that of the other serotypes (9, 10). Thus, antibodies that bind across different dimers and rafts may lose potency, depending on the temperature and strain

of DENV2. Therefore, antibodies binding to “simpler” epitopes, such as monomers or dimers, may be more effective against this serotype.

In areas of high dengue endemicity, a potential therapeutic needs to be protective in the presence of preexisting antibodies (14). Certain MAb LALA variants protect therapeutically against an ADE infection, because they are neutralizing and at the same time suppress the enhancing potential of preexisting fusion loop antibodies by displacing their binding (15–17). In contrast, highly neutralizing DIII MAbs that do not block fusion loop enhancing antibodies protect in high-dose-DENV2-lethal, but not ADE-DENV2-lethal challenge (Fig. 1C) (17). The increased efficacy of HMAb 2D22 may be due to its ability to lock E proteins and also block the binding of low-affinity fusion-loop enhancing antibodies.

The molecular features of the 2D22 epitope and the ability of HMAb 2D22-LALA to prevent ADE will aid in the development of vaccines and therapeutics, respectively.

REFERENCES AND NOTES

1. S. Bhatt *et al.*, *Nature* **496**, 504–507 (2013).
2. S. J. Thomas, T. P. Endy, *Curr. Opin. Infect. Dis.* **24**, 442–450 (2011).
3. S. B. Halstead, *Adv. Virus Res.* **60**, 421–467 (2003).
4. L. Villar *et al.*, *N. Engl. J. Med.* **372**, 113–123 (2015).
5. M. R. Capeding *et al.*, *Lancet* **384**, 1358–1365 (2014).
6. R. de Alwis *et al.*, *Proc. Natl. Acad. Sci. U.S.A.* **109**, 7439–7444 (2012).
7. X. Zhang *et al.*, *Nat. Struct. Mol. Biol.* **20**, 105–110 (2013).
8. R. J. Kuhn *et al.*, *Cell* **108**, 717–725 (2002).
9. G. Fibriansah *et al.*, *J. Virol.* **87**, 7585–7592 (2013).
10. X. Zhang *et al.*, *Proc. Natl. Acad. Sci. U.S.A.* **110**, 6795–6799 (2013).
11. G. Fibriansah *et al.*, *EMBO Mol. Med.* **6**, 358–371 (2014).
12. E. P. Teoh *et al.*, *Sci. Transl. Med.* **4**, 139ra83 (2012).

13. A. Rouvinski *et al.*, *Nature* **520**, 109–113 (2015).
14. B. R. Murphy, S. S. Whitehead, *Annu. Rev. Immunol.* **29**, 587–619 (2011).
15. S. J. Balsitis *et al.*, *PLOS Pathog.* **6**, e1000790 (2010).
16. J. D. Brien *et al.*, *J. Virol.* **87**, 7747–7753 (2013).
17. K. L. Williams *et al.*, *PLOS Pathog.* **9**, e1003157 (2013).

ACKNOWLEDGMENTS

We thank S. Shresta (La Jolla Institute for Allergy and Immunology, La Jolla, CA) and E.-E. Ooi (Duke–National University of Singapore Graduate Medical School) for providing DENV2 strains S221 and PVP94/07, respectively. The data presented in this paper are tabulated in the main paper and in the supplementary materials. Coordinates of 4°C-2D22-PVP94/07, 37°C-2D22-PVP94/07 and BF-37°C-2D22-NGC class II were deposited in the Protein Data Bank under accession codes 4UIF, 5A1Z, and 4UIH, respectively. The cryo-EM maps of 4°C-2D22-PVP94/07, 37°C-2D22-PVP94/07, 4°C-2D22-NGC, BF-37°C-2D22-NGC Class I, BF-37°C-2D22-NGC Class II, AF-37°C-2D22-NGC Class I, and AF-37°C-2D22-NGC Class II were deposited in the Electron Microscopy Database under accession numbers EMD-2967, EMD-2996, EMD-2997, EMD-2999, EMD-2968, EMD-2998, and EMD-2969, respectively. This study was supported by Ministry of Education Tier 3 (R-1913-301-146-112) grants awarded to S.-M.L., U.S. NIH grant U54 AI057157 awarded to J.E.C., NIH (National Institute of Allergy and Infectious Diseases) grant R01 AI107731 awarded to A.M.D.S. and J.E.C., NIH grant K08 AI103038 awarded to S.A.S., and grant U54 AI063359 awarded to E.H. We acknowledge the Cryo-Electron Microscopy Facility at the Center for Bio-imaging Science, Department of Biological Science, National University of Singapore for their scientific and technical assistance.

SUPPLEMENTARY MATERIALS

www.sciencemag.org/content/349/6243/88/suppl/DC1
Materials and Methods
Supplementary Text
Figs. S1 to S13
Tables S1 and S2
References (18–36)

6 February 2015; accepted 27 May 2015
10.1126/science.aaa8651

SELENOPROTEINS

CRL2 aids elimination of truncated selenoproteins produced by failed UGA/Sec decoding

Hsiu-Chuan Lin,^{1,2} Szu-Chi Ho,¹ Yi-Yun Chen,³ Kay-Hooi Khoo,^{2,3} Pang-Hung Hsu,⁴ Hsueh-Chi S. Yen^{1,2*}

Selenocysteine (Sec) is translated from the codon UGA, typically a termination signal. Codon duality extends the genetic code; however, the coexistence of two competing UGA-decoding mechanisms immediately compromises proteome fidelity. Selenium availability tunes the reassignment of UGA to Sec. We report a CRL2 ubiquitin ligase-mediated protein quality-control system that specifically eliminates truncated proteins that result from reassignment failures. Exposing the peptide immediately N-terminal to Sec, a CRL2 recognition degron, promotes protein degradation. Sec incorporation destroys the degron, protecting read-through proteins from detection by CRL2. Our findings reveal a coupling between directed translation termination and proteolysis-assisted protein quality control, as well as a cellular strategy to cope with fluctuations in organismal selenium intake.

The canonical genetic code includes 20 amino acids. Additionally, selenocysteine (Sec/U) and pyrrolysine (Pyl/O) are the 21st and 22nd amino acids and are coded by the otherwise termination codons UGA and

UAG, respectively (1, 2). Sec is cotranslationally incorporated into selenoproteins, a distinct set of proteins largely functioning as oxidoreductases, with Sec in the active sites (3–5). At least 25 selenoproteins have been identified in humans

(6). Translating UGA into Sec requires a Sec insertion sequence (SECIS) element in the 3' untranslated region (3'UTR) of mRNA transcripts, Sec-transfer RNA (tRNA), Sec-specific elongation factor (eEFSec), and the SECIS-binding protein SBP2 (7–10). This renders UGA/Sec redefinition failure-prone, facing competition between Sec-tRNA and the release factor for UGA decoding (11). The reassignment efficiency is greatly influenced by dietary selenium (12). Stop codon reprogramming expands the genetic code at the risk of introducing premature translational termination due to missed stop codon reassignment. Cells process potentially detrimental truncated proteins produced from failed UGA-to-Sec translation via previously undetermined mechanisms.

We developed GPS, a cell-based system for measuring global protein stability (13). In this system, the expression cassette contains a single promoter with an internal ribosome entry site, permitting the expression of two fluorescent proteins from one mRNA transcript. The

first fluorescent protein, RFP (red fluorescent protein), is the internal control, whereas the second fluorescent protein GFP (green fluorescent protein) is fused to the N terminus of the protein of interest. The GFP/RFP ratio is a surrogate for protein stability measurements reading the relative steady-state abundance of GFP-fusion protein over RFP (13, 14). Coupling GPS with functional ablation of ubiquitin ligase, we generated a generic platform to isolate ubiquitin ligase substrates (14, 15). This strategy identified 102 substrates for the CRL2 ubiquitin ligase, including the five selenoproteins SEPHS2, SELV, SEPX1/MSRB1, SELK, and SELS/VIMP from a GPS library containing 15,483 human open reading frames (ORFs) (fig. S1, A and B). We subcloned these selenoprotein genes into backgrounds resembling native transcripts (+UTR, Fig. 1D). Inhibition of CRL2 activity by either genetic perturbation or pharmacological treatment stabilized these selenoproteins, but not their paralogs without Sec (SEPHS1 and SEPW2) (Fig. 1A and fig. S1, C and D). The stability of selenoproteins was positively correlated with selenium availability (Fig. 1B); selenium supplementation attenuated CRL2-mediated selenoprotein degradation (Fig. 1C).

The five selenoproteins identified share no sequence similarity (fig. S1E). We generated

various selenoprotein mutants to uncover the determinants for their degradation (Fig. 1D). Analysis of selenoprotein constructs exclusively expressing truncated proteins (Δ UTR, Δ , UAA, and UAG) and those producing only full-length (FL) proteins via replacement of UGA to other codons, revealed that CRL2 selectively targeted truncated but spared FL selenoproteins (Fig. 1, E and F, and fig. S2, A and B).

We asked whether CRL2 is responsible for removing prematurely terminated selenoproteins arising from failures in UGA/Sec reprogramming. FL selenoproteins were more stable than truncated ones (Fig. 2A); the stability of selenoproteins expressed from the UTR construct fell in between, as expected from a mixture of FL and truncated proteins. Indeed, two populations of proteins were translated from the UTR-containing mRNAs upon CRL2 suppression: a shorter product terminated at the UGA codon and a longer read-through product, with the former as the only CRL2 substrate (Fig. 2B). Similar to FL selenoproteins created by substituting the UGA codon (Fig. 1, E and F), Sec-containing FL selenoproteins were stable and exempted from CRL2 surveillance (Fig. 2C and fig. S2C). Selenium availability had no effect on the stability of truncated or FL selenoproteins (fig. S2D). Rather, it enhanced the efficiency of

¹Institute of Molecular Biology, Academia Sinica, Taiwan. ²Genome and Systems Biology Degree Program, National Taiwan University, Taiwan. ³Institute of Biological Chemistry, Academia Sinica, Taiwan. ⁴Department of Life Science, Institute of Bioscience and Biotechnology, National Taiwan Ocean University, Taiwan.
*Corresponding author, E-mail: hyen@imb.sinica.edu.tw

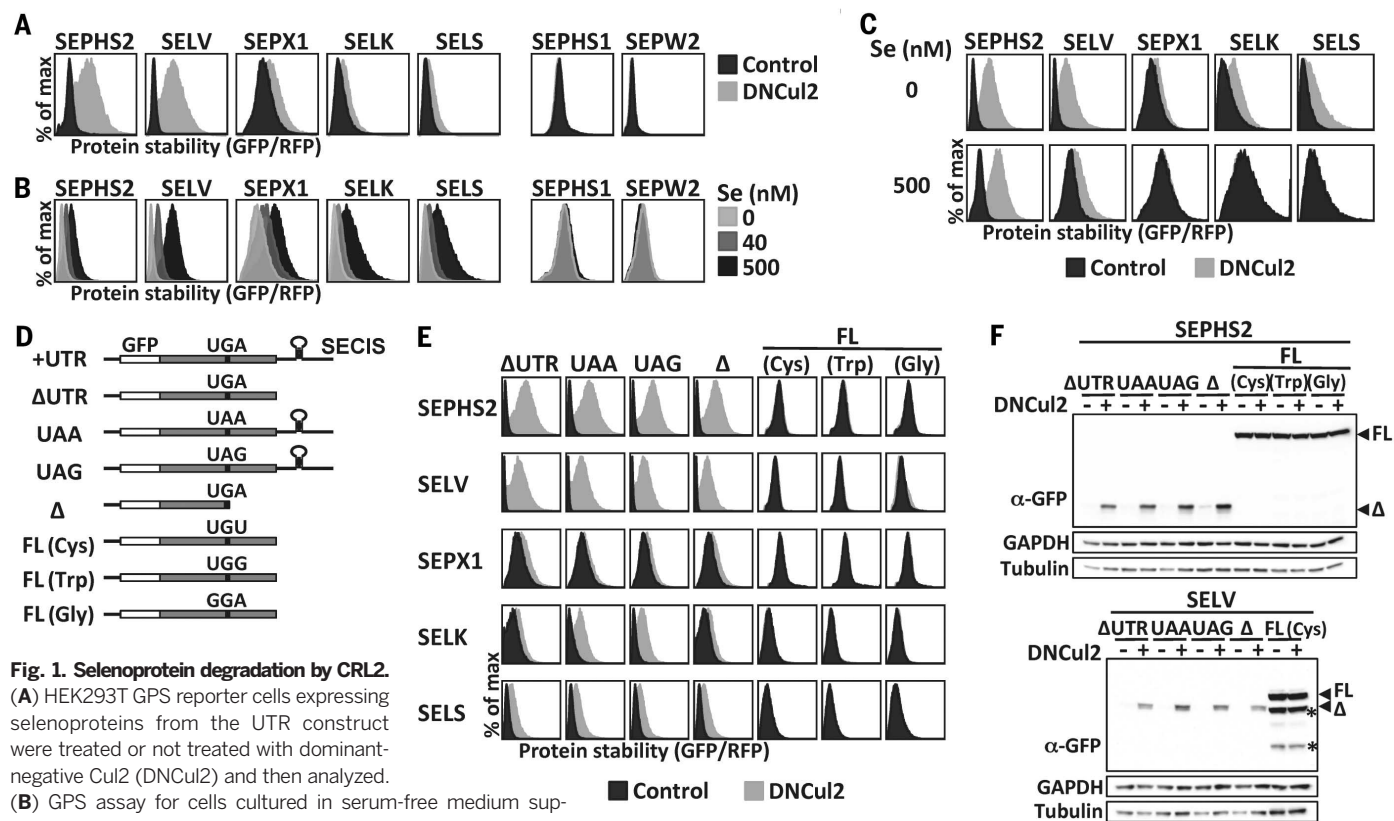


Fig. 1. Selenoprotein degradation by CRL2.

(A) HEK293T GPS reporter cells expressing selenoproteins from the UTR construct were treated or not treated with dominant-negative Cul2 (DNCu2) and then analyzed. (B) GPS assay for cells cultured in serum-free medium supplemented with various concentrations of sodium selenite. (C)

GPS assay for cells cultured in serum-free medium with or without sodium selenite supplementation and DNCu2 treatment. (D) A schematic representation and nomenclature of each selenoprotein mutant construct. (E) GPS analysis of selenoprotein mutants in (D). FL and truncated selenoproteins are presented using different x-axis scales to avoid off-scaling. (F) Western blot analysis of SEPHS2 or SELV mutants. FL and truncated (Δ) selenoproteins are indicated by arrowheads. Asterisks mark degradation products from FL SELV. GAPDH and tubulin were loading controls.

(E) GPS analysis of selenoprotein mutants in (D). FL and truncated selenoproteins are presented using different x-axis scales to avoid off-scaling. (F) Western blot analysis of SEPHS2 or SELV mutants. FL and truncated (Δ) selenoproteins are indicated by arrowheads. Asterisks mark degradation products from FL SELV. GAPDH and tubulin were loading controls.

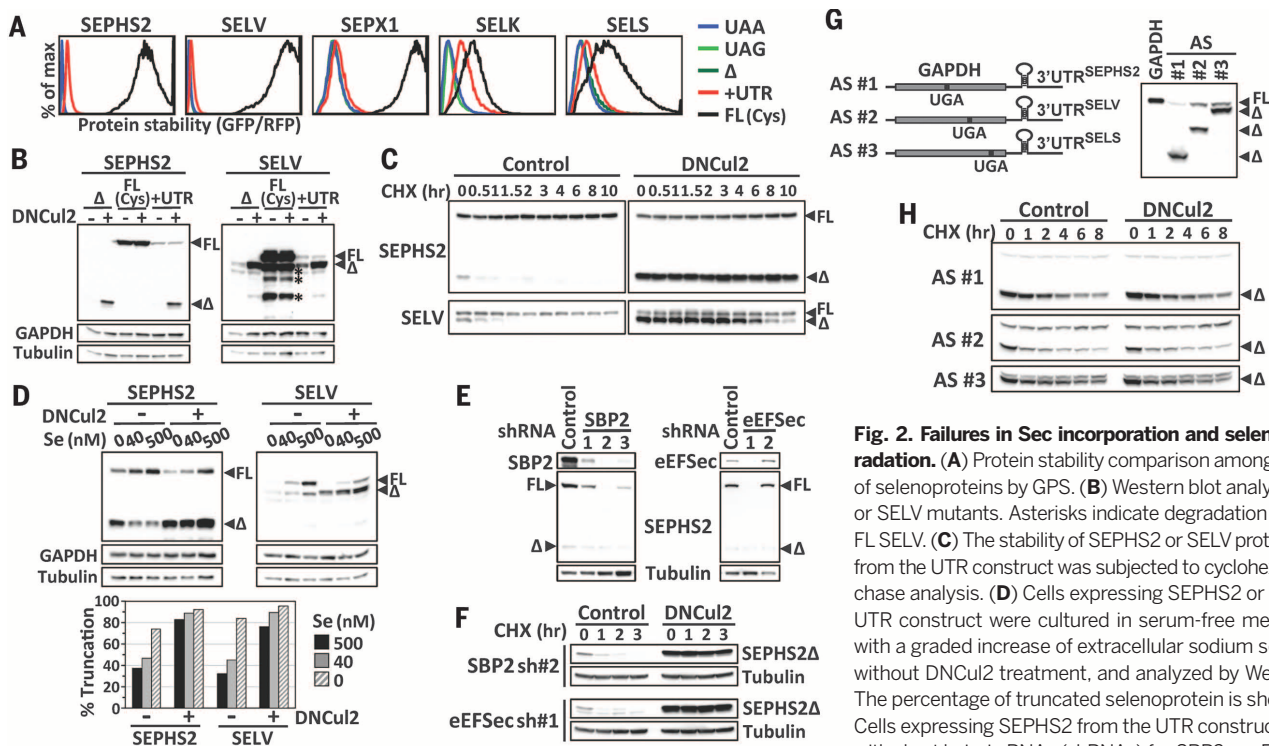


Fig. 2. Failures in Sec incorporation and selenoprotein degradation. (A) Protein stability comparison among various forms of selenoproteins by GPS. (B) Western blot analysis of SEPHS2 or SELV mutants. Asterisks indicate degradation products from FL SELV. (C) The stability of SEPHS2 or SELV proteins expressed from the UTR construct was subjected to cycloheximide (CHX)-chase analysis. (D) Cells expressing SEPHS2 or SELV from the UTR construct were cultured in serum-free medium supplied with a graded increase of extracellular sodium selenite, with or without DNCu2 treatment, and analyzed by Western blotting. The percentage of truncated selenoprotein is shown below. (E) Cells expressing SEPHS2 from the UTR construct were treated with short hairpin RNAs (shRNAs) for SBP2 or eEFSec and then analyzed by Western blotting. (F) The protein stability of SEPHS2 in cells treated with shRNAs for SBP2 or eEFSec was analyzed by CHX chase. (G) A schematic representation of GAPDH artificial selenoprotein (AS) transcripts. Cells expressing wild-type GAPDH or AS were analyzed by Western blotting. The introduced in-frame UGA codon terminated GAPDH at amino acid positions 152, 247, and 301. (H) CHX-chase analysis of GAPDH expressed from AS transcripts in (G).

analyzed by Western blotting. (F) The protein stability of SEPHS2 in cells treated with shRNAs for SBP2 or eEFSec was analyzed by CHX chase. (G) A schematic representation of GAPDH artificial selenoprotein (AS) transcripts. Cells expressing wild-type GAPDH or AS were analyzed by Western blotting. The introduced in-frame UGA codon terminated GAPDH at amino acid positions 152, 247, and 301. (H) CHX-chase analysis of GAPDH expressed from AS transcripts in (G).

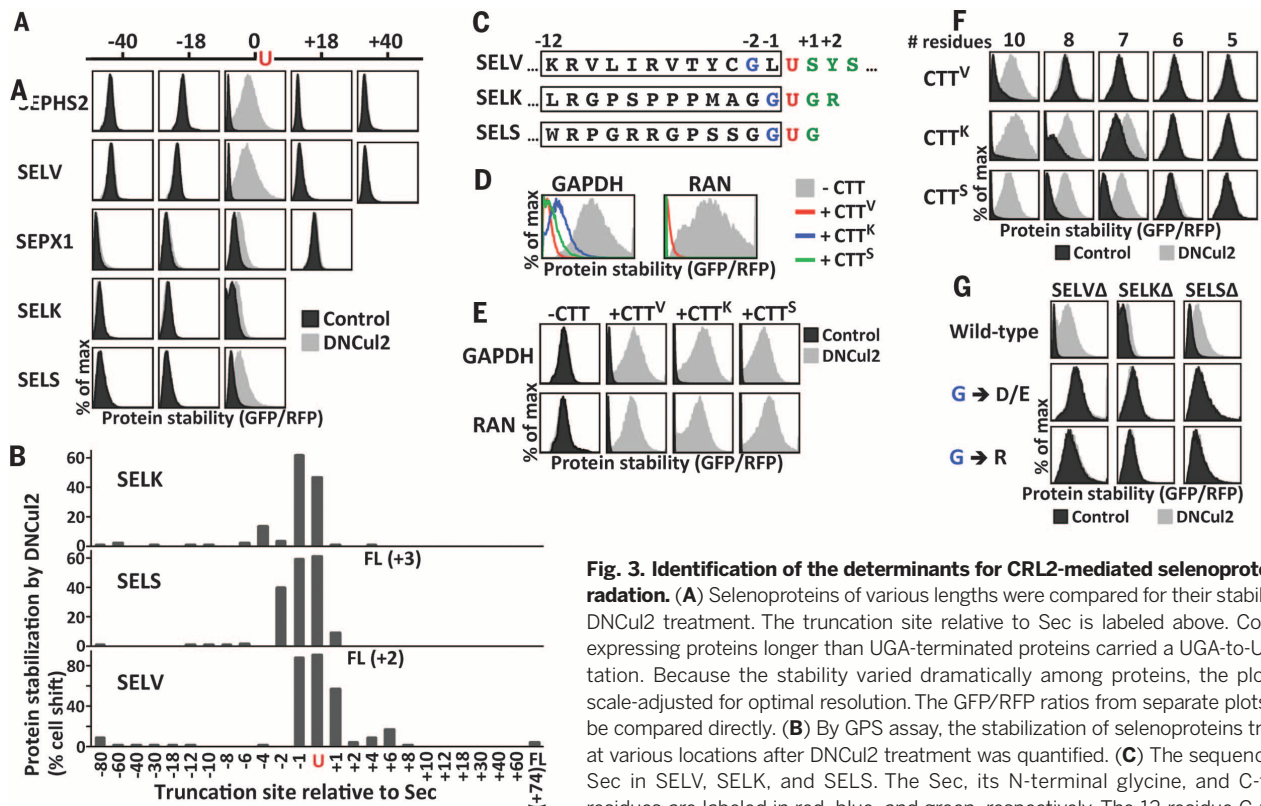


Fig. 3. Identification of the determinants for CRL2-mediated selenoprotein degradation. (A) Selenoproteins of various lengths were compared for their stability upon DNCu2 treatment. The truncation site relative to Sec is labeled above. Constructs expressing proteins longer than UGA-terminated proteins carried a UGA-to-UGU mutation. Because the stability varied dramatically among proteins, the plots were scale-adjusted for optimal resolution. The GFP/RFP ratios from separate plots cannot be compared directly. (B) By GPS assay, the stabilization of selenoproteins truncated at various locations after DNCu2 treatment was quantified. (C) The sequences near Sec in SELV, SELK, and SELS. The Sec, its N-terminal glycine, and C-terminal residues are labeled in red, blue, and green, respectively. The 12-residue C-terminal truncation (CTT) is marked with a box. (D to E) The protein stability of GAPDH or RAN without or with CTT tags at the C terminus was analyzed. CTT^V, CTT^K, and CTT^S, represent the CTT of SELVΔ, SELKΔ, and SELSΔ, respectively. (F) The stability of GAPDH tagged with various lengths of CTTs. (G) The stability of UGA-terminated selenoproteins with mutations in the glycine N-terminal to Sec.

Sec insertion (Fig. 2D). The accumulation of truncated selenoproteins was heightened by CRL2 inhibition, regardless of the selenium supplies (Fig. 2D and fig. S2E). Endogenously made truncated selenoproteins were accumulated upon CRL2 inhibition (fig. S3). Taken together, these results reveal a role of CRL2 as a gatekeeper in selenoprotein quality control.

CRL2 can recognize truncated SELK and SELS, even though these two proteins differ from their FL counterparts by only three or two amino acids, respectively (fig. S1E). CRL2 may recognize truncated selenoproteins by sensing incomplete translation via scouting the UTR of mRNA transcripts. Alternatively, components in Sec incorporation machinery may assist CRL2 to distinguish UGA-terminated selenoproteins. However, selenoproteins expressed from constructs lacking 3'UTRs or sequences 3' to UGA remained CRL2 substrates (Fig. 1, E and F). Pro-

tein half-lives of truncated selenoproteins from transcripts with or without 3'UTR were comparable (fig. S4A). Moreover, knocking down SBP2 or eEFSec, which are trans-acting elements essential for Sec incorporation, decreased Sec insertion efficiency but did not influence CRL2-mediated degradation (Fig. 2, E and F). To examine whether CRL2-mediated degradation exhibits substrate specificity, we created artificial selenoproteins; CRL2 could not target UGA-terminated glyceraldehyde phosphate dehydrogenase (GAPDH) made from GAPDH transcripts with in-frame UGA codons within the ORF and 3'UTR from authentic selenoproteins (Fig. 2, G and H). Collectively, our data support the notion of direct recognition of truncated protein products by CRL2.

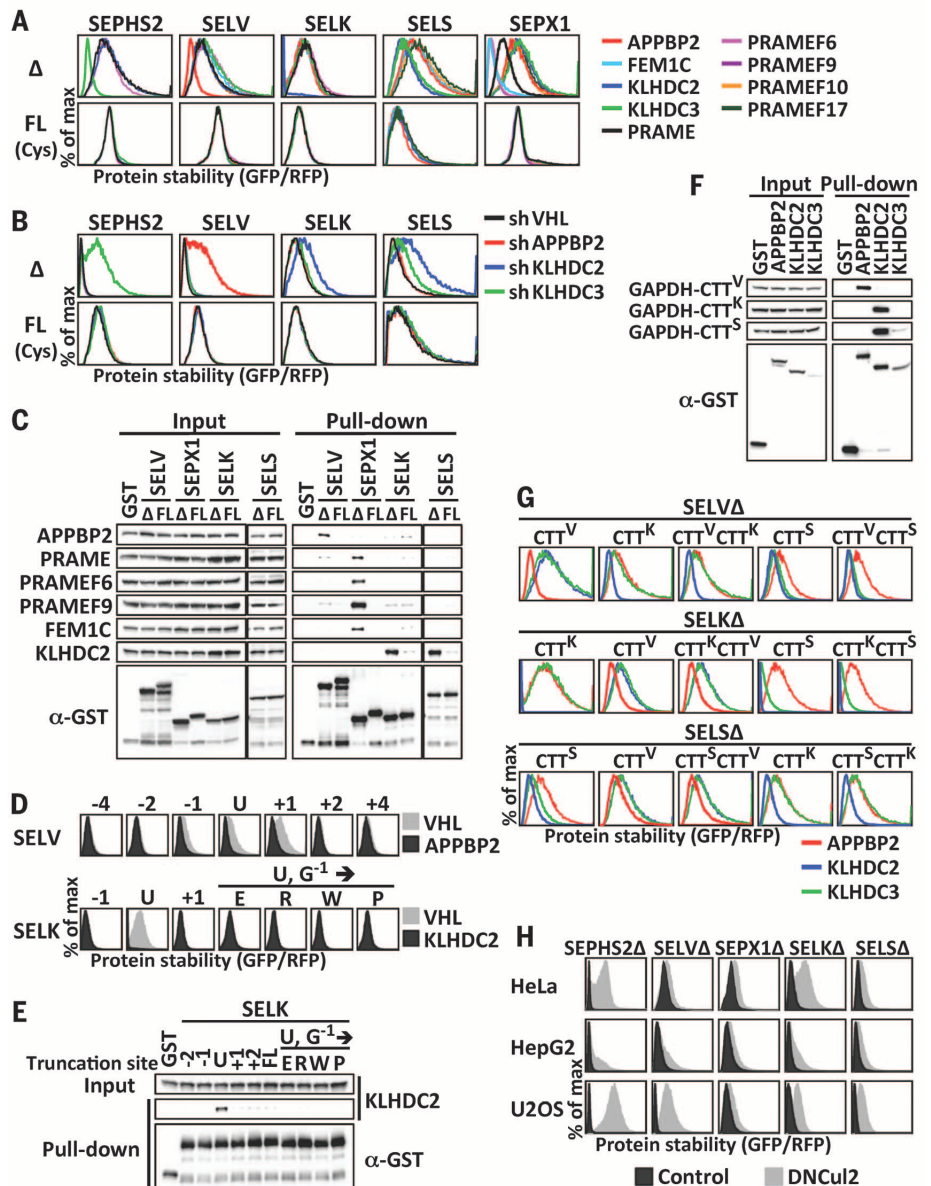
We systematically shortened (-) or extended (+) the length of the UGA-terminated selenoprotein (Δ) to elucidate how CRL2 recognized

truncated selenoproteins. Truncations had to be made at the position within one to two amino acid residues originally translated into Sec so as to promote CRL2-mediated degradation (Fig. 3, A and B, and fig. S4B). A 12-residue C-terminal tail (CTT) of UGA-terminated selenoproteins was sufficient to promote CRL2-mediated degradation (Fig. 3C and fig. S5, A and B). Fusion of CTTs to GAPDH and RAN, which are not natural CRL2 substrates, resulted in their degradation by CRL2 (Fig. 3, D and E). Thus, CTTs comprise transferable CRL2 degrons (degradation signals). The minimal CRL2 degrons can be as small as 10 or 7 residues in length (Fig. 3F).

We identified a critical glycine at the -1 position of SELK and SELS, or at the -2 position of SELV (Fig. 3C). Replacing this glycine with other amino acids abolishes CRL2-dependent degradation (Fig. 3G and fig. S5B). Changing the leucine at the -1 position of SELV, next to

Fig. 4. The BC-box proteins contribute to CRL2 recognition of truncated selenoproteins.

(A) GPS assay for cells carrying UGA-terminated (Δ) or FL selenoproteins infected with viruses expressing various BC-box proteins. (B) GPS assay for cells expressing Δ or FL selenoproteins treated with shRNAs against BC-box proteins. FL and Δ selenoproteins were presented using different x-axis scales. (C) GST pull-down using lysates expressing hemagglutinin (HA)-tagged BC-box proteins and GST or GST-tagged Δ or FL selenoproteins. (D) GPS assay for cells expressing various forms of SELV or SELK infected with viruses expressing VHL, APPBP2, or KLHDC2. The truncation sites relative to Sec are labeled above. (E) GST pull-down using lysates expressing HA-tagged KLHDC2 and GST or various forms of GST-tagged SELK. (F) GST pull-down using lysates expressing GFP-tagged GAPDH-CTT fusion and GST or GST-tagged BC-box proteins. (G) The protein stability of truncated selenoproteins terminated with various CTTs. (H) The stability of UGA-terminated selenoproteins in various cells.



this glycine, did not affect SELV degradation (fig. S5C). The residues C-terminal to Sec, covering the degron, can tolerate more extreme replacement (fig. S5D). Fusing the C-terminal end of UGA-terminated selenoproteins to GFP fully abrogated selenoprotein degradation (fig. S5E). An illegitimate C terminus, once exposed, triggers CRL2-mediated selenoprotein quality control. Rather than serving as a general inspector to eliminate every abnormal selenoproteins, CRL2 mediates the degradation to clear truncated translational products of unsuccessful UGA-to-Sec decoding.

CRL2 is a modular ubiquitin ligase that uses an interchangeable set of BC-box proteins as substrate receptors when forming approximately 40 different CRL2 complexes with a host of substrate specificities (16–19). We found that CRL2 targeted various UGA-terminated selenoproteins via distinct BC-box proteins (Fig. 4, A and B, and fig. S6). KLHDC3, APPBP2, and KLHDC2 were used to target SEPHS2, SELV and SELK, respectively; SELS could be targeted by both KLHDC2 and KLHDC3. SEPX1 could be recognized by four BC-box proteins, namely PRAME, PRAMEF6, PRAMEF9, and FEMIC. Each BC-box protein was preferentially associated with the corresponding UGA-terminated selenoprotein over the FL one (Fig. 4C and fig. S6, D and E). Furthermore, the substrate selectivity of CRL2 was attributed to BC-box proteins (Fig. 4, D and E). Supporting the idea that CTTs comprise CRL2 degrons, GAPDH-CTT fusions confer binding to the acceptor BC-box proteins (Fig. 4F). Swapping respective BC-box proteins can be achieved by exchanging CTTs or adding an extra CTT C-terminal to UGA-terminated selenoprotein (Fig. 4G and fig. S7A).

In examining the prevalence of proteolysis-assisted selenoprotein quality control, we detected CRL2-mediated quality surveillance for SEPHS2, SELV, SEPX1, SELK, and SELS in all cell types tested (Fig. 4H and fig. S8A). We surveyed six additional selenoproteins and identified one more CRL2 substrate, SEPW1. CRL2 also selectively degraded the UGA-terminated version of SEPW1 while sparing the read-through version (fig. S8B). Regardless of the involvement of CRL2, FL selenoproteins were more stable than their truncated counterparts, and truncated proteins were degraded by the ubiquitin-proteasome pathway (fig. S8, C and D).

When selenium is limited, the transcripts of some, but not all, selenoproteins are driven toward degradation by the nonsense-mediated mRNA decay pathway (20–22). CRL2 provides an additional layer of defense against translational errors due to the duality in codon assignment. The tiered and complementary nature of these two safeguards grants robustness and fidelity to selenoprotein quality control. Here we report a mechanism by which CRL2 recognizes aberrant selenoproteins via various substrate receptors. We have allocated the peptide immediately N-terminal to Sec as the CRL2-targeting degron triggering degradation when placed at the C-terminal end of a protein (fig. S9A). The

CRL2 degrons are highly conserved across species (fig. S9B). The BC-box proteins responsible for selenoprotein recognition do not share common substrate recognition motifs. Instead, they contain various structural motifs involved in general protein-protein interaction, such as Kelch, LRR, ANK, and TPR repeats (fig. S7B). APPBP2, KLHDC2, KLHDC3, PRAME, and FEMIC have all been implicated in human diseases, although selenoproteins are their only identified substrates to date. Beyond exclusively serving as selenoprotein-specific inspectors, these CRL2 substrate receptors may play a broader role in targeted protein degradation.

REFERENCES AND NOTES

1. A. Ambrogelly, S. Palioura, D. Söll, *Nat. Chem. Biol.* **3**, 29–35 (2007).
2. A. V. Lobanov, A. A. Turanov, D. L. Hatfield, V. N. Gladyshev, *Crit. Rev. Biochem. Mol. Biol.* **45**, 257–265 (2010).
3. S. R. Lee *et al.*, *Proc. Natl. Acad. Sci. U.S.A.* **97**, 2521–2526 (2000).
4. D. L. Hatfield, V. N. Gladyshev, *Mol. Cell. Biol.* **22**, 3565–3576 (2002).
5. L. Zhong, A. Holmgren, *J. Biol. Chem.* **275**, 18121–18128 (2000).
6. G. V. Kryukov *et al.*, *Science* **300**, 1439–1443 (2003).
7. L. V. Papp, J. Lu, A. Holmgren, K. K. Khanna, *Antioxid. Redox Signal.* **9**, 775–806 (2007).
8. D. M. Driscoll, P. R. Copeland, *Annu. Rev. Nutr.* **23**, 17–40 (2003).
9. D. L. Hatfield, B. A. Carlson, X. M. Xu, H. Mix, V. N. Gladyshev, *Prog. Nucleic Acid Res. Mol. Biol.* **81**, 97–142 (2006).
10. J. Donovan, P. R. Copeland, *Antioxid. Redox Signal.* **12**, 881–892 (2010).
11. A. Mehta, C. M. Rebsch, S. A. Kinzy, J. E. Fletcher, P. R. Copeland, *J. Biol. Chem.* **279**, 37852–37859 (2004).

12. M. T. Howard, B. A. Carlson, C. B. Anderson, D. L. Hatfield, *J. Biol. Chem.* **288**, 19401–19413 (2013).
13. H. C. Yen, Q. Xu, D. M. Chou, Z. Zhao, S. J. Elledge, *Science* **322**, 918–923 (2008).
14. M. J. Emaniuele *et al.*, *Cell* **147**, 459–474 (2011).
15. H. C. Yen, S. J. Elledge, *Science* **322**, 923–929 (2008).
16. N. Mahrouf *et al.*, *J. Biol. Chem.* **283**, 8005–8013 (2008).
17. T. Kamura *et al.*, *Genes Dev.* **18**, 3055–3065 (2004).
18. F. Okumura, M. Matsuzaki, K. Nakatsukasa, T. Kamura, *Front. Oncol.* **2**, 10 (2012).
19. M. D. Petroski, R. J. Deshaies, *Nat. Rev. Mol. Cell Biol.* **6**, 9–20 (2005).
20. R. A. Sunde, A. M. Raines, K. M. Barnes, J. K. Evenson, *Biosci. Rep.* **29**, 329–338 (2009).
21. A. Seyedal, M. J. Berry, *RNA* **20**, 1248–1256 (2014).
22. X. Sun *et al.*, *Mol. Biol. Cell* **12**, 1009–1017 (2001).

ACKNOWLEDGMENTS

We thank H. H. Chuang, M. D. Tsai, C. H. Yeang, L. Y. Chen, J. Y. Leu, and A. Pena for suggestions; Y. F. Chen, P. Y. Hsieh, T. T. Lee, S. Y. Lin, C. Y. Tai, and M. C. Tsai for technical assistance; S. J. Elledge, D. E. Hill, and M. Vidal for reagents. The CRL2 GPS screen was initiated at S.J.E.'s laboratory and completed in H.C.Y.'s laboratory. Orbitrap data were acquired at the Academia Sinica Common Mass Spectrometry Facilities located at the Institute of Biological Chemistry. This work was supported by Career Development Award 101-CDA-L05 from Academia Sinica and Ministry of Science and Technology (MOST) grant 103-2311-B-001-034-MY3 awarded to H.C.Y., MOST grant 102-2113-M-019-003-MY2 to P.H.H., and NIH grant AG011085 to S.J.E.

SUPPLEMENTARY MATERIALS

www.sciencemag.org/content/349/6243/91/suppl/DC1
Materials and Methods
Figs. S1 to S9

4 March 2015; accepted 3 June 2015
10.1126/science.aab0515

STRUCTURAL VIROLOGY

Conformational plasticity of a native retroviral capsid revealed by x-ray crystallography

G. Obal,^{1,2*} F. Trajtenberg,^{3*} F. Carrión,¹ L. Tomé,^{1,2†} N. Larrioux,³ X. Zhang,⁴ O. Pritsch,^{1,2†} A. Buschiazzi^{3,5†}

Retroviruses depend on self-assembly of their capsid proteins (core particle) to yield infectious mature virions. Despite the essential role of the retroviral core, its high polymorphism has hindered high-resolution structural analyses. Here, we report the x-ray structure of the native capsid (CA) protein from bovine leukemia virus. CA is organized as hexamers that deviate substantially from sixfold symmetry, yet adjust to make two-dimensional pseudo-hexagonal arrays that mimic mature retroviral cores. Intra- and interhexameric quasi-equivalent contacts are uncovered, with flexible trimeric lateral contacts among hexamers, yet preserving very similar dimeric interfaces making the lattice. The conformation of each capsid subunit in the hexamer is therefore dictated by long-range interactions, revealing how the hexamers can also assemble into closed core particles, a relevant feature of retrovirus biology.

Retroviruses undergo an obligatory maturation step in the formation of infectious particles (1–3). The cleavage of Gag generates several mature proteins, including capsid (CA), which self-assembles into a

fullerene-like core, enclosing the RNA genome. Revealing the molecular features of the retroviral mature core and its assembly mechanism is important for understanding retrovirus biology and developing novel antiretroviral drugs.

This copy is for your personal, non-commercial use only.

If you wish to distribute this article to others, you can order high-quality copies for your colleagues, clients, or customers by [clicking here](#).

Permission to republish or repurpose articles or portions of articles can be obtained by following the guidelines [here](#).

The following resources related to this article are available online at www.sciencemag.org (this information is current as of July 5, 2015):

Updated information and services, including high-resolution figures, can be found in the online version of this article at:

<http://www.sciencemag.org/content/349/6243/91.full.html>

Supporting Online Material can be found at:

<http://www.sciencemag.org/content/suppl/2015/07/01/349.6243.91.DC1.html>

This article **cites 21 articles**, 13 of which can be accessed free:

<http://www.sciencemag.org/content/349/6243/91.full.html#ref-list-1>

This article appears in the following **subject collections**:

Biochemistry

<http://www.sciencemag.org/cgi/collection/biochem>